

Ibrahim Tinni Tahiru
Doctoral Researcher

School of Environmental Sciences
University of Liverpool
L69 3GP

T 07 459 618180
E ibrahim.tahiru@liverpool.ac.uk

25 December 2023

COVER SHEET

Dear Editors,

This manuscript has been sent for consideration for publication in Journal of Sedimentary Research (JSR) special edition. We think this is a concise report of exciting research results that will be of interest to a broad range of Earth Scientists interested to understand more about the architecture of submarine fans, for example, whether hierarchy as interpreted by several authors occur in submarine fans. We have adopted a reduced complexity numerical modelling approach because this allows exploration of the simplest-case processes allowing us to build fundamental understanding of how strata accumulate and record Earth-surface process signals.

Please note that, despite having undergone peer-review, the manuscript has yet to be formally accepted for publication. Subsequent version of this manuscript may have slightly different content. If accepted, the final version of this manuscript will be available via the 'Peer-reviewed Publication DOI' link on the right-hand side of this webpage. Please feel free to contact any of the authors; we welcome feedback.

Yours sincerely,



Ibrahim Tinni Tahiru

Journal of Sedimentary Research

Deep-Water Fan Hierarchy: Assumptions, Evidence, and Numerical Modelling Analysis --Manuscript Draft--

Manuscript Number:	
Article Type:	Bouma Conference
Corresponding Author:	Ibrahim Tinni Tahiru University of Liverpool School of Environmental Sciences Liverpool, UNITED KINGDOM
First Author:	Ibrahim Tinni Tahiru
Order of Authors:	Ibrahim Tinni Tahiru Peter Burgess Christopher Stevenson
Abstract:	<p>Submarine fan strata are commonly described and interpreted assuming a nested, hierarchical organisation of elements, from beds, to lobe elements, lobes and lobe complexes. However, describing outcrop and subsurface strata following a particular conceptual method or model is never evidence in itself that the model or method accurately reflects the true nature of the strata. To develop better understanding of and methods for robust hierarchy identification and measurement we developed two metrics, a clustering strength metric that measures how much clustering is present in the spatial distribution of beds on a submarine fan, and a hierarchy step metric that indicates how many clustered hierarchical elements are present in the bed spatial distribution. Both metrics are applied to two quantitative fan models. The first is a very simple geometric model with 10 realisations ranging from a perfectly clustered hierarchy to a indistinguishable-from-random arrangement of beds. The second model, Lobyte3D, is a reduced-complexity process model which uses a steepest descent flow routing algorithm, combined with a simple but physically reasonable representation of flow velocity, erosion, transport and deposition thresholds, to generate detailed 3D representations of submarine fan strata. Application of the cluster strength and hierarchy step metric to the simpler model demonstrates how the metrics usefully characterise how much order and hierarchy is present in the fan strata. Application to four Lobyte3D models with increasingly complex basin-floor topography shows no evidence for true hierarchy, despite clear self-organisation of the model strata into lobes, suggesting that either Lobyte3D is missing key as yet unidentified processes responsible for producing hierarchy, or that interpretations of hierarchy are not realistic.</p>

1 **Deep-Water Fan Hierarchy: Assumptions, Evidence, and Numerical Modelling**
2 **Analysis**

3

4 Ibrahim Tinni Tahiru, Peter M. Burgess and Christopher Stevenson

5 Department of Earth, Oceans and Ecological Science, University of Liverpool.

6

7

8

ABSTRACT

9 Submarine fan strata are commonly described and interpreted assuming a nested, hierarchical
10 organisation of elements, from beds, to lobe elements, lobes and lobe complexes. However,
11 describing outcrop and subsurface strata following a particular conceptual method or model is never
12 evidence in itself that the model or method accurately reflects the true nature of the strata. To
13 develop better understanding of and methods for robust hierarchy identification and measurement
14 we developed two metrics, a clustering strength metric that measures how much clustering is
15 present in the spatial distribution of beds on a submarine fan, and a hierarchy step metric that
16 indicates how many clustered hierarchical elements are present in the bed spatial distribution. Both
17 metrics are applied to two quantitative fan models. The first is a very simple geometric model with
18 10 realisations ranging from a perfectly clustered hierarchy to a indistinguishable-from-random
19 arrangement of beds. The second model, Lobyte3D, is a reduced-complexity process model which
20 uses a steepest descent flow routing algorithm, combined with a simple but physically reasonable
21 representation of flow velocity, erosion, transport and deposition thresholds, to generate detailed
22 3D representations of submarine fan strata. Application of the cluster strength and hierarchy step
23 metric to the simpler model demonstrates how the metrics usefully characterise how much order
24 and hierarchy is present in the fan strata. Application to four Lobyte3D models with increasingly
25 complex basin-floor topography shows no evidence for true hierarchy, despite clear self-organisation
26 of the model strata into lobes, suggesting that either Lobyte3D is missing key as yet unidentified
27 processes responsible for producing hierarchy, or that interpretations of hierarchy are not realistic.

28

29

30

INTRODUCTION

31 Submarine fans are among the largest sedimentary accumulations (William, 1970; Posamentier and
32 Kolla, 2003; Talling *et al.*, 2012) and serve as an essential record of Earth history, offering insights
33 into both local and global geological processes (Emmel and Curray, 1984; Pirmez and Imran, 2003;

34 Deptuck *et al.*, 2008; Picot *et al.*, 2016; Picot *et al.*, 2019; Rabouille *et al.*, 2017). Formed by a
35 complex interplay of turbidity currents, other types of sediment mass flows, and various hydraulic
36 processes, submarine fans are characterized by their complex stratigraphic architectures and
37 depositional patterns (Straub and Pyles, 2012) Submarine fans are also often important reservoirs
38 for the extraction of hydrocarbons and, increasingly importantly, for the sequestration of carbon
39 (Pettingill, Weimer and Anonymous, 2002).

40 Understanding the organization of submarine fan strata is important for unravelling their formative
41 processes and for deciphering the geological history they preserve. Previous studies have proposed
42 hierarchical schemes to describe fan internal organization and characterise spatial and temporal
43 variations in sedimentation patterns (Gardner, 2000; Pyles, 2008; Deptuck *et al.*, 2008; Prelat *et al.*,
44 2009; Prelat *et al.*, 2010) ; Mutti and Normak 1987; Gardner and Borer 2000, Pyles 2007; Deptuck
45 *et al.* 2008, Prelat *et al.*, 2009; Prelat *et al.*, 2010). However, despite the significant progress made in
46 characterizing submarine fan architecture, quantitative evidence to define hierarchy remains sparse,
47 and aspects of the fundamental mechanisms that would form hierarchical patterns remain poorly
48 defined.

49

50 **Existing Hierarchical Schemes**

51 If submarine fans are hierarchical, they should show some form of systematic pattern of smaller-
52 scale structures nested within and composing larger-scale structures. For example, in a hierarchical
53 fan, fan lobes would be composed of lobe elements that are in turn each composed of many beds,
54 each bed being one turbidite (Figure 1). Various examples of this type of hierarchical arrangement
55 have been interpreted from outcrop, and subsurface data.

56 Deptuck *et al.* (2008) used ultra-high-resolution boomer seismic imagery with a vertical resolution of
57 approximately 1 m to define a hierarchical classification for 20 lobes in a late Pleistocene submarine

58 fan offshore from East Corsica. The classification scheme defined four types of unit starting with a
59 bed or bed-set deposited from single flows, with systematic lateral compensational offsets up to 500
60 m. Bed-sets stack to form lobe elements, which, in turn, stack to create composite lobes. Composite
61 lobes are separated by disconformable surfaces, abrupt vertical shifts in acoustic facies, or the
62 presence of thin drapes, all resulting from compensational stacking of lobe-elements with lateral
63 offsets ranging from 500 to 2000 m triggered by local avulsion (Deptuck et al. 2008). Composite
64 lobes fed by the same primary conduit stack to form lobe complexes, which frequently exhibit 3-5km
65 lateral shifts between their thickest regions, interpreted to arise from large-scale channel-mouth
66 avulsions. Abandoned composite lobes may be covered by several meters of hemipelagic drape,
67 which may subsequently be eroded by later flows.

68 Based on well-exposed Permian deposits in the Tanqua depocenter of the Karoo Basin, South Africa
69 Prelat et al. (2009) proposed a different four-fold hierarchical classification focused on the
70 properties and geometry of fine-grained interlobe architectural units, which separate more sand-
71 prone bodies. The lowest hierarchical level is single depositional event beds up to 0.5 m thick and
72 hundreds of meters wide. Lobe elements up to 5m thick are composed of stacked beds and form the
73 next higher hierarchical level. Genetically linked vertically stacked lobe elements, separated by fine-
74 grained units typically less than 2 cm thick but occasionally up to 2m thick in topographic lows,
75 create lobes up to 5 m thick with widths exceeding 20 km. Finally, lobe complexes are composed of
76 stacked lobe bodies, up to 50 m thick and 40 km wide fed by a single upstream channel.

77 Macdonald *et al.*, (2011) focused on the process sedimentology and internal architecture of lobe
78 deposits in the Carboniferous Ross Sandstone Formation, to propose a three-order hierarchy of bed-
79 sets, lobe-elements, and composite lobes. Lobe-elements are formed by upward-thickening
80 packages of bed-sets, often with basal mudstone units indicative of depositional shutdown.
81 Mudstone thicknesses relate to the lateral distance and duration of avulsion separating
82 compensationally-stacked lobe-elements.

83 (Cullis *et al.*, 2018) systematically reviewed and compared a representative selection of the most
84 widely adopted deep-marine hierarchy schemes, to assess the principal characteristics of each
85 hierarchical classification, the common diagnostic criteria used to attribute deposits to given
86 hierarchical orders, and the causes of similarity and variability between different schemes. The
87 review revealed recurrent observations underlying all the classification schemes, recommended that
88 hierarchical relationships be categorised based on primary sedimentological observations, rather
89 than through predefined schemes and concluded that a universal process-based hierarchy cannot be
90 established. This is because of the difficulty in to reconcile the different hierarchical schemes arising
91 partly from differences between the underlying studies such as the data types, scales of interest,
92 specific environmental settings and in the significance given to the diagnostic criteria, as well as from
93 the adoption of non-standard terminology.

94 Straub and Pyle (2012) used a modified version of the compensation index to test for statistically
95 significant differences in compensation between different scales in hierarchically-classified strata.
96 They also examined compensation variations between predominantly channelized and
97 unchannelized submarine fan strata in each hierarchical class to test how compensation varies
98 spatially. Their results suggest that hierarchical divisions based on compensation are justified, and
99 that compensation increases along a longitudinal transect through distributive submarine fans.

100

101 **Numerical Stratigraphic Forward Modelling as a Tool for Analysis of Submarine Fan Hierarchy**

102 Numerical stratigraphic forward modelling has emerged as a useful tool for unravelling the
103 complexities of sedimentary system (Paola, 2000; Burgess, 2013). By simulating the interplay
104 between sediment transport, deposition, and erosion processes, these models provide valuable
105 insights into the formation of stratigraphic patterns. Reduced-complexity models aim to capture the
106 simplest possible set of processes that may be responsible for a specific stratigraphic pattern, while

107 also reducing computational cost, allowing multiple model runs and intensive analysis of model
108 results, in this case to explore the emergence of hierarchical patterns within submarine fan systems.
109 This study utilizes the reduced-complexity stratigraphic forward model, Lobyte3D version 2.2, to
110 investigate the hierarchical organization of submarine fan deposits. Lobyte3D is a three-dimensional
111 reduced-complexity numerical stratigraphic forward model, developed to help understand how and
112 why stacking patterns evolve in submarine fan depositional systems (Burgess *et al.*, 2019). Lobyte3D
113 has been modified from its original form with new representations of key depositional processes,
114 and most importantly, the addition of erosion as a function of flow velocity (Mackie et al., in review).
115 In this paper Lobyte3D is used examine the architecture of submarine strata to to (1) access if there
116 is any definite criteria to interpret lobes and (2) describe patterns present within each lobes. And (3)
117 perform clustering analysis on the flow centroid to quantitatively identify and define lobes.

118

119

MODEL FORMULATION AND METHODOLOGY

120 **Lobyte3D Formulation**

121 Lobyte3D version 2.2 calculates turbidity flow routing, erosion and deposition, and the resulting
122 stacking patterns that evolve as sediment accumulates on a submarine-fan surface. Transport and
123 deposition are calculated on a simple orthogonal 50 by 50 km x-y grid with a cell edge dimension of
124 100m. Each model run consisted of 1000 flow events. Sediment enters the model at y0 at the top of
125 a submarine slope. All the sediment volume in one flow event is moved downslope as one single
126 depth-averaged packet of sediment in one model grid cell at each iteration following a steepest
127 gradient descent down the slope. Deposition starts in the cell where depth-averaged flow velocity
128 into the lowest adjacent cell is equal to or less than a specified sediment threshold velocity. Flow
129 velocity is calculated such that.

130

$$v_f = v_i + (a * \emptyset) \quad (1)$$

131 where V_f is the flow velocity, V_i is the velocity of the flow at the previous time step, a is the flow
132 acceleration and ϕ is the flow acceleration proportion taken to be 0.5

133 The flow acceleration a is given by.

$$134 \quad a = v_m - v_i \quad (2)$$

135 and the maximum velocity V_m converts shear velocity into whole flow velocity as a function of
136 topographic gradient and is given by

$$137 \quad v_m = \frac{v_s}{\sqrt{\sigma}} \quad (3)$$

138 where V_s is the maximum shear velocity and σ is the basal friction coefficient.

139 Flow erosion rate is calculated as

$$140 \quad \varepsilon_r = v_{se} * \frac{a}{b} \quad (4)$$

141 where v_{se} is the settling velocity and a and b can be calculated as

$$142 \quad a = C_e * Z^5 \quad (5)$$

$$143 \quad b = 1 + \frac{C_e}{0.3} * Z^5 \quad (6)$$

144 where C_e is the erosion rate constant, and Z is the tractive stress which is calculated as follows.

$$145 \quad Z = Re^6 * \frac{v_s}{v_{se}} \quad (7)$$

146 where R_e is the particle Reynold number.

147 Four scenarios of Lobyte3D with varying degrees of complexity in the initial topography was used to
148 model 1000 flow events. They include concave flat floor with no noise, very smoothed noise,
149 smoothed noise, and raw noise. Each flow interrupts background hemipelagic deposition occurring
150 at a rate of 0.02 m ky^{-1} . A flow repeat time of 1000 years will be maintained through each model run

151 representing a 1 My of flow history and deposition. Input parameters for the model include the initial
 152 topography, distribution of the grain-size, deposition threshold velocity to commence dispersive
 153 flow and deposition, concentration of the sediment, total volume of sediment transported by the
 154 flows (Table1).

155 For each model run, model behaviour was analysed by plotting each down-slope flow route and area
 156 of deposition in map view. Avulsion points were identified when the apex of flow deposition shifted
 157 substantially from the location of the apex of the previous flow.

158 Table 1: Lobyte3D input parameters

S/N	Parameter	Value
1	Hemipelagic deposition rate, per time step, m My ⁻¹	0.02
2	Diffusion coefficient, m ² per My.	0.0
3	Density (kg/m ³) of the ambient fluid	1.00
4	Erosion rate constant (m/s)	1.3 x 10 ⁻¹⁰
5	Basal friction coefficient	0.004
6	D50 (m) median grain diameter (medium/fine sand)	0.00025
7	Grain density in kg/m ³ siliciclastic quartz/feldspar	2660
8	Depositional velocity threshold (m/s) to commence dispersive flow and deposition	0.1
9	Flow acceleration/deceleration coefficient	0.5
10	Total flow thickness, fluid and sediment mix (m)	100
11	Flow COG proportion	0.10

12	Volumetric sediment concentration	0.01
13	Minimum flow thickness (m)	0.001
14	Proportion of the height of ponding topographic lows to fill when flow is trapped	1.00
15	Flow Radiation Factor	2.0
16	Number of fractions in the depositional fraction profile	13

159

160 **Clustering Analysis and Hierarchy Metrics**

161 Clustering analysis is a numerical technique to classify data, originally developed as a natural
162 sciences method to make taxonomy more objective. (Everitt *et al.*, 2011), but now widely applied in
163 earth sciences (Simpson, Thatcher and Savage, 2012; Takahashi *et al.*, 2019) to identify patterns,
164 group similar objects, and uncover underlying structures within data. Cluster analysis partitions data
165 based on their similarities or dissimilarities, and often provides valuable insights into the
166 organization and relationships within the data (Everitt *et al.*, 2011). Clustering, unlike other
167 classification techniques, does not rely on preset classes and class-labelled samples, so is a relatively
168 more objective method (Jiawei Han, 2011).

169 Data point separation distances, or dissimilarity, are a fundamental aspect of many clustering
170 analyses, quantified using a wide range of dissimilarity measures (Gower and Legendre, 1986), often
171 in matrix form. Dissimilarity matrices capture pairwise dissimilarities, the distances between
172 individual data points, such that

173

$$D = \begin{bmatrix} 0 & & & & & \\ d(2,1) & 0 & & & & \\ d(3,1) & d(3,2) & 0 & & & \\ \vdots & \vdots & \vdots & & & \\ d(n,1) & d(n,2) & \cdots & \cdots & 0 & \end{bmatrix}$$

174 Where $d(i, j)$ is the measured dissimilarity between objects i and j . since $d(i, j) = d(j, 1)$, and
 175 $d(i, i) = 0$. Analysis of a dissimilarity matrix allows distinction between randomly distributed data
 176 where a broad spread of dissimilarity distances is expected, and clustered data, where the distances
 177 have a narrower range of values reflecting the specific distances within and between clusters; in
 178 clustered data, many of the dissimilarity distances are relatively small because many points occur in
 179 close proximity within the clusters.

180 Here we use a metric termed clustering strength to distinguish between clustered xyz data, and a
 181 randomly distributed set of xyz points. Clustering strength is calculated from the centroid separation
 182 distances such that

183

$$CSI = \left(\sum_{i=1}^N I(d_i \leq T) \right) / N$$

184 where N is the number of bed centroids, d_i is the separation distance between centroid point i and
 185 another centroid, T is a threshold distance, and I is an indicator function that returns 1 if or 0,
 186 depending the logical condition $d_i \leq T$. For a threshold distance that is 1% of the maximum
 187 dissimilarity distance in the system, values of clustering strength will approach zero as the degree of
 188 randomness in xyz points increase, and the value will always be higher for clustered data.

189 Once a degree of non-random clustering has been identified, the nature of the clustering can be
 190 assessed, specifically whether there is any hierarchical element such that smaller clusters
 191 themselves cluster to form larger clusters, and so on (e.g. Figure 1). Hierarchical Agglomerative
 192 Clustering Analysis (Gordon, 1987) is a bottom-up clustering analysis approach that starts with
 193 individual data points, merging them into new clusters based on their dissimilarity values, until all

194 points are within one cluster. Euclidean dissimilarity distances were used because these most
195 effectively measure bed centroid spatial relationships in xyz coordinate space, and the complete
196 linkage method was selected because it has low sensitivity to outliers, and is relatively robust in
197 noisy data (Jiawei Han, 2011), so a good choice to identify hierarchy levels.

198 Hierarchical cluster analysis results are plotted as a dendrogram, with cluster separation distance on
199 the Y-axis, and cluster number on the x-axis. The actual degree of hierarchy present in the
200 dendrogram can be assessed quantitatively by extracting dissimilarity distances between
201 dendrogram bifurcation points, and analysing these for clustering also; a hierarchical example should
202 show clustering in these bifurcation distances, because bifurcations should occur at specific scales
203 reflecting the size and separation distance of the various hierarchical elements. The hierarchy step
204 metric is then the number of distinct clusters identified in the dendrogram bifurcation point
205 distances, typically 1 for indistinguishable from random points with little or no clustering, and
206 otherwise a number representing the number of hierarchical levels present in the data.

207

208

RESULTS

209 Synthetic Lobe Model Results

210 To provide a well-understood definitively hierarchical baseline for the analysis, eleven synthetic fan
211 lobe models were constructed and analysed, each comprising 1000 beds, with 40 beds in a lobe
212 element, five lobe elements per lobe, and five lobes in total. These models are range from perfectly
213 deterministic and hierarchical, with distinct lobes and lobe elements composed of beds arranged in a
214 simple retrogradational stacking pattern, to a completely stochastic example with a stochastic
215 distribution of bed centroids (Figure 2). The entirely deterministic fan arrangement follows the three
216 or four-fold hierarchy described in (Gervais *et al.*, 2006; Deptuck *et al.*, 2008; Prelat, Hodgson and
217 Flint, 2009) (Figure 1). A random offset is added to each x and y coordinate in the deterministic

218 model, and the magnitude of the added random element ranges from 0.05 to 0.5. For example, a
219 model with a random element of 0.2 has a random offset of each x and y coordinate ranging from -
220 0.1 to 0.1.

221 For each synthetic fan lobe model, cluster strength was calculated, and also hierarchy step values
222 were derived from dendrogram analysis (Figure 3). The cluster strength values range from a high of
223 5.7×10^{-3} for the completely deterministic hierarchically clustered fan, to 1.0×10^{-5} for the entirely
224 random bed centroid points, and the decrease in the metric value is quite sharp as the magnitude of
225 random point offset increases (Figure 4A). The dendrogram hierarchy analysis shows a similar
226 pattern. The two least-random-component models yield a hierarchy step value of 3, an accurate
227 measurement of the number of hierarchical levels built in to each model (Figure 4B). In contrast, the
228 models with a random offset value of 0.2 and greater have a hierarchy step value of 1 indicating that
229 a random offset of 0.2 or more is enough to remove any detectable hierarchy.

230

231 **Lobyte3D Model Results**

232 Lobyte3D was run with four different initial topographies defining scenarios with no noise, very
233 smoothed noise, smoothed noise, and raw noise. Strike-oriented cross-sections, 3D views of the
234 channel, bed and lobe stacking patterns, and bed centroid maps from these different initial
235 topographies are used to understand how variations in initial topography control avulsion, fan
236 stacking, and the hierarchical organization of the modelled submarine fan strata.

237 *Avulsion Cycle Processes*

238 The avulsion process is key to forming lobes and therefore key to generating any stratal hierarchy
239 present, so it is important to understand exactly how avulsion occurs in the model. Evolving flow
240 routing shows substantial changes during avulsion, bypassing previous mounded depositional
241 topography, and cutting a new section of channel that bypasses sediment further into the basin to

242 the point where the initial basin floor slope is low enough to decelerate the flow enough to trigger
243 deposition.

244 Analysis of the first avulsion in the no noise case reveals the detail of how avulsion occurs in
245 Lobyte3D. Prior to flow 190, deposition was backstepping up the basin-margin slope, partially
246 backfilling the mouth of the previously cut channel (Figure 5). Upslope backstepping occurred due to
247 flow interaction at the channel-lobe transition, with strata deposited from previous flows triggering
248 flow deceleration and further deposition. As strata backstep upslope, depositional relief at the
249 channel mouth on the proximal mound edge increased, and magnitude of deceleration when flows
250 reach this depositional topography also increased. Each time a flow encounters a mound that has
251 been built by previous flows, the flow will continue to follow the steepest available down-slope
252 route, and therefore tend to divert left or right to climb over the lowest-relief part of the mound.
253 Flow velocity prior to climbing the depositional mound tends to increase through time as deposition
254 backsteps up the basin-margin slope, and by flow 190, the flow had sufficient remaining velocity
255 after climbing the depositional mound (Figure 5) to continue to flow, accelerate down from the crest
256 of the mound, and start to cut a new channel. Flow routing through the new channel bypasses the
257 positive topography produced by the previous lobe deposition, defines a new route further into the
258 basin (Figure 5b), and starts to deposit a new lobe, defining an avulsion event.

259 Rather obviously this is a much-simplified representation of what actually happens in deep-water
260 depositional systems. For instance, several processes have been investigated to produce instability
261 that results in avulsion-threshold circumstances. Channel sinuosity, channel lengthening, channel
262 thalweg and levee aggradation, and channel-relief reduction are some of these causes (Kolla, 2007;
263 Prelat, Hodgson and Flint, 2009; Groenenberg *et al.*, 2010). In this analysis we assume that this
264 modelled avulsion process is sufficiently realistic and representative enough of the real physical
265 process to form the basis for at least initial numerical experiment exploration of how this behaviour
266 influences fan lobe geometry stacking and potential hierarchy.

267

268 *Flow Routing and Stacking Patterns*

269 All four modelled scenarios generated a multi-km-scale submarine fan (Figure 7) consisting of
270 interbedded turbidite event beds and background hemipelagic strata organised as more-or-less
271 discrete lobes (Figure 8) broadly comparable to typical observed submarine-fan bathymetry and
272 successions (Romans *et al.*, 2009; Romans *et al.*, 2011; Prelat, Hodgson and Flint, 2009; Prelat and
273 Hodgson, 2013). The no noise initial topography produces the most systematic lobe stacking with a
274 simple compensational stacking pattern and lobe boundaries clearly defined by a few meters of
275 hemipelagic sediments (Figure 8A). Each lobe is composed of around 60-to-200 mostly contiguous,
276 spatially-clustered backstepping flow events. Lobes have a simple stacking pattern, separated by
277 progressive lateral 1-2km shift in focus of deposition, and a mean duration of 114 ky (Figure 8A).

278 The very smooth noise initial topography produces similar but slightly more complex lobe stacking
279 pattern (Figure 8B). These lobes consist of around 50 to 130 aggradational and backstepping beds
280 with a lateral lobe separation distance of 2-4 km and a mean duration of 83 ky (Figure 8B, Figure 9B).

281 The smooth noise initial topography case still shows some discrete lobes, but lobe structure and
282 stacking are more complex (Figure 7C). Where distinct enough to measure, lobes consist of 35-70
283 contiguous spatially clustered flow events, with lateral lobe separation distance ranging from 0.5 to
284 2 km and a mean duration of 50 ky (Figure 8C, Figure 9C). Finally, the raw noise initial topography
285 shows the most complex lobe stacking pattern lacking any clear trend (Figure 7D, Figure 9D). These
286 lobes are even more difficult to define. Where discrete enough to define, lobes consist of 5 to 270
287 aggradational and backstepping stacked beds with a separation distance of 1 to 3 km, but also the
288 highest gradual lateral shift within each lobe (Figure 8D) and a mean duration of 112 ky.

289

290 *Quantification of Clustering and Hierarchy in Lobby3D Results*

291 Cluster strength values for the four Lobyte3D models range from 2.51×10^{-3} to 1.14×10^{-3} (Figure 4A)
292 and the smoothed noise initial topography generates the highest clustering strength, suggesting that
293 smoothed noise in the basin-floor topography can enhance clustering relative to the case with the
294 simplest no-noise topography. In contrast, the raw noise basin-floor topography model has the
295 lowest clustering strength (Figure 4A) due to the irregular topography disrupting the regular stacking
296 and avulsion pattern required for clustering. All four model runs generate strata with a hierarchical
297 step value of 1, indicating that no hierarchy is detectable in the spatial distribution of bed centroids,
298 despite the clustering. This suggests that although the clustering produces clear lobe structures,
299 particularly in the no noise and smoothed noise cases, this bed-lobe distinction is not enough to
300 define a hierarchy measured by this dendrogram-derived metric.

301

302

DISCUSSION

303 **Reduced complexity models**

304 Reduced complexity models are, by design, very much simplified representations of the complex
305 processes that generate real strata (Liang et al., 2015). Consequently, results from reduced
306 complexity models must be used carefully, and not over interpreted or assumed to have predictive
307 power beyond what is reasonably supported by their constituent process representations. However,
308 these models also have some substantial advantages over more complex models, particularly their
309 lower computational cost, and perhaps most importantly, the fact that if a reduced complexity
310 model demonstrates a particular emergent behaviour, the process representation in the model is
311 quite likely to be the simplest possible representation of that process.

312 In this case Lobyte3D shows avulsion events that divert deposition into new locations clustering sets
313 of beds to form lobes. Critical elements in the model necessary for this a steepest-descent transport
314 algorithm and a gradient threshold for initiation for turbidite bed deposition. Both these elements

315 are represented in a very simple but physically reasonable way, and do seem to operate to some
316 degree in real submarine fan systems. Given this the resulting lobe formation in the model is
317 probably realistic enough to offer some basic but useful insight in deep-water fan processes and
318 structure. However, it is also important to remember that additional and more realistic
319 representations of key processes, for example more detail in the 3D structure and spatial
320 distribution of each flow and consideration of a range of grain sizes in each flow may generate
321 different avulsion process and different fan structures (e.g. (Wahab *et al.*, 2022)) and (Hamilton,
322 Strom and Hoyal, 2015) found that uneven topography increases channel avulsion likelihood due to
323 localized variations in sediment concentration, leading to mouth bar formation and hydraulic jumps.
324 Clearly these processes and controls require further investigation with more complex models, but
325 starting with the simplest model seems sensible.

326

327 **Influence of initial topography**

328 Lobyte3D models in this analysis show substantial influence of initial topography on flow routing,
329 avulsion, and lobe stacking patterns. Previous studies have shown or interpreted a similar influence
330 of topography in shaping submarine fan evolution and architecture (Groenenberg *et al.*, 2010;
331 Straub and Pyles, 2012; Hamilton, Strom and Hoyal, 2015; Cullis *et al.*, 2018; Ferguson *et al.*, 2020);
332 taken together these results support the hypothesis that initial topography influences lobe switching
333 and avulsion timing (Piper and Normark, 2001; Gervais *et al.*, 2006; Groenenberg *et al.*, 2010;
334 Ferguson *et al.*, 2020). However, the formulation of Lobyte3D is perhaps particularly sensitive to
335 small changes in seafloor topography, especially in terms of flow routing prior to deposition, so
336 further work developing more complex model formulations or testing this effect with other
337 numerical and analogue models is required.

338

339 **Absence of hierarchy**

340 There is no hierarchy present in these Lobyte3D results; all modelled strata show detectable non-
341 random clustering, as indicated by comparison with the entirely synthetic fan models, but all the
342 Lobyte3D models have a hierarchical step value 1. This combination of cluster and hierarchy metric
343 values indicate that no hierarchy is detectable in the spatial distribution of bed centroids, despite
344 the clustering.

345 Clearly absence of a hierarchy in strata calculated in a reduced complexity numerical model is not
346 necessarily evidence that hierarchy does not occur in real deep-water fan strata. However, nor is
347 interpretation of outcrop and subsurface data following a conceptual model of stratal hierarchy
348 evidence that the deep-water fan strata really are hierarchical. Failure to reproduce hierarchy in a
349 very simple numerical model highlights two end-member possibilities; either hierarchy is a real
350 feature of deep-water fan strata, but occurs by processes not adequately represented in Lobyte3D,
351 or the interpretations of hierarchy in outcrop and subsurface strata are an over-interpretation of
352 limited data with insufficient quantitative evidence to be properly robust.

353 Avulsion is a key control on hierarchy formation because it is the main process forming clustered
354 entities such as lobes. Avulsion in Lobyte3D happens in a simplified and specific way that likely does
355 not capture the range of different and perhaps more complex mechanisms that operate in real
356 submarine fan systems (Hamilton *et al.*, 2015; Ortiz-Karpf *et al.*, 2015; Qi *et al.*, 2022; de Haas *et al.*,
357 2016). Clearly therefore further modelling and model development is required, with Lobyte3D or
358 other process models including analogue models perhaps, to explore how other avulsion processes
359 might behave differently and produce hierarchical clustering.

360 Until now, interpretations of hierarchy in submarine fan strata have been mostly qualitative, and this
361 lack of quantitative evidence does mean that conclusions of hierarchy are much more tenuous than
362 has perhaps been recognised. More quantitative analysis is therefore required, but a key challenge is
363 how to analyse limited data, for example one-dimensional vertical sections, to provide metrics that

364 can reliably identify and present or absence of hierarchy developed in three-dimensional strata;
365 most current interpretations do not recognise or account for this uncertainty (Gervais et al. 2006;
366 Deptuck et al. 2008; Prelat et al. 2009; MacDonald et al. 2011), suggesting that hierarchical patterns
367 observed in previous studies are probably not universally applicable to all submarine fan systems
368 (Cullis et al. 2018; Ferguson et al. 2020), and development of further tools for quantification of
369 hierarchy with limited outcrop and subsurface data is essential.

370

371

CONCLUSIONS

372 1. Submarine fan strata are commonly described and interpreted to have a nested, hierarchical
373 organisation of elements, but quantitative evidence from outcrop and subsurface data to
374 support this interpretation is limited.

375 2. Two new metrics are defined, calculated and used to identify the degree of hierarchy
376 present in the modelled fan strata. A clustering strength metric measures how much
377 clustering is present in the spatial distribution of Lobyte3D beds, and a hierarchy step metric
378 indicates how many clustered hierarchical elements are present in the bed spatial
379 distribution.

380 3. Both metrics applied to a definitively hierarchical geometric fan model with ten
381 progressively more randomised realisations, shows that the combined metrics can clearly
382 distinguish between hierarchical and non-hierarchical realisations.

383 4. The combined metrics also show that there is no hierarchy present in the four Lobyte3D
384 realisations, suggesting that either Lobyte3D is missing key as yet unidentified processes
385 responsible for producing hierarchy, or that hierarchal interpretations of outcrop and
386 subsurface data are more complicated and less realistic than typically assumed.

387

388

389

390

- 392 Burgess, P. M. (2013) 'CarboCAT: A cellular automata model of heterogeneous carbonate strata',
393 *Computers & geosciences*, 53, pp. 129-140.
- 394 Burgess, P. M., Masiero, I., Toby, S. C. and Duller, R. A. (2019) 'A big fan of signals? Exploring
395 autogenic and allogenic process and product in a numerical stratigraphic forward model of
396 submarine-fan development', *Journal of sedimentary research*, 89(1), pp. 1-12.
- 397 Cullis, S., Colombera, L., Patacci, M. and McCaffrey, W. D. (2018) 'Hierarchical classifications of the
398 sedimentary architecture of deep-marine depositional systems', *Earth-science reviews*, 179, pp. 38-
399 71.
- 400 de Haas, T., van den Berg, W., Braat, L., Kleinhans, M. G. and Mohrig, D. (2016) 'Autogenic avulsion,
401 channelization and backfilling dynamics of debris flow fans', *Sedimentology*, 63(6), pp. 1596-1619.
- 402 Deptuck, M. E., Piper, D. J. W., Savoye, B. and Gervais, A. (2008) 'Dimensions and architecture of late
403 Pleistocene submarine lobes off the northern margin of east Corsica', *Sedimentology*, 55(4), pp. 869-
404 898.
- 405 Emmel, F. J. and Curray, J. R. (1984) 'The Bengal submarine fan, Northeastern Indian Ocean', *Geo-
406 marine letters*, 3(2-4), pp. 119-124.
- 407 Everitt, B. S., Landau, S., Leese, M. and Stahl, D. (2011) *Cluster Analysis. Wiley series in probability
408 and statistics* 5. Aufl. edn. Newark: Wiley.
- 409 Ferguson, R. A., Kane, I. A., Eggenhuisen, J. T., Pohl, F., Tilston, M., Spychala, Y. T. and Brunt, R. L.
410 (2020) 'Entangled external and internal controls on submarine fan evolution: an experimental
411 perspective', *The depositional record*, 6(3), pp. 605-624.
- 412 Gervais, A., Savoye, B., Mulder, T. and Gonthier, E. (2006) 'Sandy modern turbidite lobes; a new
413 insight from high resolution seismic data', *Marine and petroleum geology*, 23(4), pp. 485-502.
- 414 Gordon, A. D. (1987) 'A Review of Hierarchical Classification', *Journal of the Royal Statistical Society.
415 Series A. General*, 150(2), pp. 119-137.
- 416 Gower, J. C. and Legendre, P. (1986) 'Metric and Euclidean properties of dissimilarity coefficients',
417 *Journal of classification*, 3(1), pp. 5-48.
- 418 Groenenberg, R. M., Hodgson, D. M., Prelat, A., Luthi, S. M. and Flint, S. S. (2010) 'Flow-deposit
419 interaction in submarine lobes; insights from outcrop observations and realizations of a process-
420 based numerical model', *Journal of sedimentary research*, 80(3), pp. 252-267.
- 421 Hamilton, P. B., Strom, K. B. and Hoyal, D. C. J. D. (2015) 'Hydraulic and sediment transport
422 properties of autogenic avulsion cycles on submarine fans with supercritical distributaries', *Journal
423 of geophysical research. Earth surface*, 120(7), pp. 1369-1389.

424 Jiawei Han, J. P. M. K. (2011) *Data Mining: Concepts and Techniques. The Morgan Kaufmann Series in*
425 *Data Management Systems* 2nd Edition edn.: Elsevier Science.

426 Kolla, V. (2007) 'A review of sinuous channel avulsion patterns in some major deep-sea fans and
427 factors controlling them', *Marine and petroleum geology*, 24(6-9), pp. 450-469.

428 Macdonald, H. A., Peakall, J., Wignall, P. B. and Best, J. (2011) 'Sedimentation in deep-sea lobe-
429 elements; implications for the origin of thickening-upward sequences', *Journal of the Geological*
430 *Society*, 168(2), pp. 319-332.

431 Michael H. Gardner, J. M. B. (2000) 'Abstract: Submarine channel architecture along a slope to basin
432 profile, Brushy Canyon Formation, West Texas', *AAPG bulletin*, 84 (2000).

433 Ortiz-Karpf, A., Hodgson, D. M. and McCaffrey, W. D. (2015) 'The role of mass-transport complexes
434 in controlling channel avulsion and the subsequent sediment dispersal patterns on an active margin:
435 The Magdalena Fan, offshore Colombia', *Marine and petroleum geology*, 64, pp. 58-75.

436 Paola, C. (2000) 'Quantitative models of sedimentary basin filling', *Sedimentology*, 47(s1), pp. 121-
437 178.

438 Pettingill, H. S., Weimer, P. and Anonymous (2002) 'Worldwide deepwater exploration and
439 production; past, present, and future', *Leading edge (Tulsa, Okla.)*, 21(4), pp. 371-376.

440 Picot, M., Droz, L., Marsset, T., Dennielou, B. and Bez, M. (2016) 'Controls on turbidite
441 sedimentation; insights from a quantitative approach of submarine channel and lobe architecture
442 (late Quaternary Congo Fan)', *Marine and petroleum geology*, 72, pp. 423-446.

443 Picot, M., Marsset, T., Droz, L., Dennielou, B., Baudin, F., Hermoso, M., de Rafelis, M., Sionneau, T.,
444 Cremer, M., Laurent, D. and Bez, M. (2019) 'Monsoon control on channel avulsions in the Late
445 Quaternary Congo Fan', *Quaternary science reviews*, 204, pp. 149-171.

446 Piper, D. J. W. and Normark, W. R. (2001) 'Sandy fans; from Amazon to Hueneme and beyond', *AAPG*
447 *bulletin*, 85(8), pp. 1407-1438.

448 Pirmez, C. and Imran, J. (2003) 'Reconstruction of turbidity currents in Amazon Channel', *Marine and*
449 *petroleum geology*, 20(6), pp. 823-849.

450 Posamentier, H. W. and Kolla, V. (2003) 'Seismic geomorphology and stratigraphy of depositional
451 elements in deep-water settings', *Journal of sedimentary research*, 73(3), pp. 367-388.

452 Preal, A., Covault, J. A., Hodgson, D. M., Fildani, A. and Flint, S. S. (2010) 'Intrinsic controls on the
453 range of volumes, morphologies, and dimensions of submarine lobes', *Sedimentary geology*, 232(1-
454 2), pp. 66-76.

455 Preal, A. and Hodgson, D. M. (2013) 'The full range of turbidite bed thickness patterns in submarine
456 lobes; controls and implications', *Journal of the Geological Society*, 170(1), pp. 209-214.

457 Prelat, A., Hodgson, D. M. and Flint, S. S. (2009) 'Evolution, architecture and hierarchy of distributary
458 deep-water deposits; a high-resolution outcrop investigation from the Permian Karoo Basin, South
459 Africa', *Sedimentology*, 56(7), pp. 2132-2154.

460 Pyles, D. R. (2008) 'Multiscale stratigraphic analysis of a structurally confined submarine fan;
461 Carboniferous Ross Sandstone, Ireland', *AAPG bulletin*, 92(5), pp. 557-587.

462 Qi, K., Gong, C., Steel, R. J., Shao, D., Ding, L. and Ma, H. (2022) 'The formation and development of
463 avulsions and splays of submarine channel systems: Insights from 3D seismic data from the
464 northeastern Bengal Fan', *Sedimentary geology*, 440, pp. 106239.

465 Rabouille, C., Baudin, F., Dennielou, B. and Olu, K. (2017) 'Organic carbon transfer and ecosystem
466 functioning in the terminal lobes of the Congo deep-sea fan: outcomes of the Congolobe project',
467 *Deep-sea research. Part II, Topical studies in oceanography*, 142(2), pp. 1-6.

468 Romans, B. W., Fildani, A., Hubbard, S. M., Covault, J. A., Fosdick, J. C. and Graham, S. A. (2011)
469 'Evolution of deep-water stratigraphic architecture, Magallanes Basin, Chile', *Marine and petroleum
470 geology*, 28(3), pp. 612-628.

471 Romans, B. W., Normark, W. R., McGann, M. M., Covault, J. A. and Graham, S. A. (2009) 'Coarse-
472 grained sediment delivery and distribution in the Holocene Santa Monica Basin, California;
473 implications for evaluating source-to-sink flux at millennial time scales', *Geological Society of
474 America bulletin*, 121(9-10), pp. 1394-1408.

475 Simpson, R. W., Thatcher, W. and Savage, J. C. (2012) 'Using cluster analysis to organize and explore
476 regional GPS velocities', *Geophysical research letters*, 39(18), pp. n/a.

477 Straub, K. M. and Pyles, D. R. (2012) 'Quantifying the hierarchical organization of compensation in
478 submarine fans using surface statistics', *Journal of sedimentary research*, 82(11), pp. 889-898.

479 Takahashi, A., Hashimoto, M., Hu, J. C., Takeuchi, K., Tsai, M. C. and Fukahata, Y. (2019) 'Hierarchical
480 Cluster Analysis of Dense GPS Data and Examination of the Nature of the Clusters Associated With
481 Regional Tectonics in Taiwan', *Journal of geophysical research. Solid earth*, 124(5), pp. 5174-5191.

482 Talling, P. J., Masson, D. G., Sumner, E. J. and Malgesini, G. (2012) 'Subaqueous sediment density
483 flows: Depositional processes and deposit types', *Sedimentology*, 59(7), pp. 1937-2003.

484 Wahab, A., Hoyal, D. C., Shringarpure, M. and Straub, K. M. (2022) 'A dimensionless framework for
485 predicting submarine fan morphology', *Nature communications*, 13(1), pp. 7563-7563.

486 William, R. N. (1970) 'Growth Patterns of Deep-Sea Fans', *AAPG bulletin*, 54.

487

488

489

490 **Figure captions**

491 Figure 1: An idealised model of hierarchical stacking patterns with three primary clusters each
492 defining a lobe, and each further subdivided into four lobe-element sub-clusters, each of which is
493 composed of a series of individual turbidite beds.

494 Figure 2: Centroid plot of synthetic fan models, with a normalised 0-to-1 xy coordinate range, and
495 varying degrees of randomness in the bed centroid xy coordinates A. Totally deterministic and
496 hierarchical, without random offset, B. moderate randomness with a random element of 0.1, C.
497 significant randomness with a random element of 0.5. D. Totally random model with a random
498 element of 1.0. As randomness increases from 0 to 1, the distinction between clusters diminishes,
499 reflecting a transition from well-defined, hierarchical patterns, to a random arrangement of beds.

500 Figure 3. Dendograms calculated from a selection of synthetic fan scenarios. A. Totally deterministic
501 and hierarchical model. B. Synthetic model with a random offset of 0.2. C. Synthetic model with a
502 random offset of 0.5. D. Totally stochastic model with a random offset

503 Figure 4. Measurements of clustering and hierarchy in the synthetic fan models. A. Cluster strength
504 plotted against the maximum random point separation shows that cluster strength decreases
505 sharply from a maximum with no random element in the synthetic fan model, to much lower values
506 for a maximum random offset of 0.1 and greater. B. The hierarchy step metric shows 3 hierarchical
507 levels for maximum random offsets less than 0.1, and only one level, so no evidence of hierarchy, for
508 greater levels of randomness in the synthetic fan models.

509 Figure 5. Topography from the no noise model showing the lobe (yellow), channel, and sediment
510 flow paths (blue) for pre-avulsion flow 189 (a) and post-avulsion flow 190 (b) at the avulsion node
511 location. Yellow cells indicate the location of deposition of the previous flow. Flow 189 deposits a
512 small part of its sediment load at the channel mouth, diverts and climbs over previously-deposited
513 topography, and decelerates and deposits. Flow 190, in contrast, deposits, ascends, but retains
514 enough velocity to divert, accelerate, and start cutting a new channel, defining a new route to begin
515 to deposit a new lobe.

516 Figure 6. Plot of the no-noise model topography (solid lines) and flow velocity (dashed lines) versus
517 flow distance along the route of flows 189 (red lines) and 190 (blue lines). Prior to avulsion, flow 189
518 velocity first reverses sign as it hits an opposite-facing slope on previous depositional mound
519 topography, deposits some sediment in the channel mouth that accretes to the back of the previous
520 depositional mound, then decelerates to near zero velocity climbing the prior topography, below the
521 threshold velocity for continued transport, at which point full flow deposition commences. In
522 contrast, flow 190 has sufficient velocity on the slightly steeper slope such that flow deceleration
523 climbing the mound is insufficient to trigger deposition, leaving sufficient remaining velocity to flow
524 over the mound crest, accelerate down the mound lee slope, and start cutting a new channel that
525 defines a new avulsed route further into the basin.

526 Figure 7. 3D views for each of the different initial topographies, showing how successive flows in
527 different colours backstep up-slope to form lobes, and then avulse as flows divert around the
528 depositional topography created by previous flows using different initial topography. A. no noise
529 topography, B. very smooth noise, C. smooth noise, and D. raw noise topography. Blue circles show
530 the apex position of each turbidite bed, so show stacking pattern of beds, which is mostly
531 aggradational with a slight retrogradational element.

532 Figure 8. Strike-oriented cross-section and chronostratigraphic plot a y = 15km, for each of the four
533 initial topographies, showing distinct packages of flow deposits each separated by a hemipelagic
534 unit. A. no noise topography, B. very smooth noise, C. smooth noise, and D. raw noise. Clustering of

535 beds is evident in all four model runs, but becomes more complex as the degree of smoothing of the
536 noise in the initial topography is reduced. Note different colours in the cross section delineate
537 turbidite beds, and triangle geometries are backfilled channels, and in the chronostratigraphic
538 diagram light blue indicates lobe deposition while pale pink indicates channel erosion.

539 Figure 9. Plot of centroids of stacked beds obtained from Lobyte3D with different initial
540 topographies. A: No noise, 3 lobes. b: very smooth noise, 4 lobes. c: smooth noise, 4 – 5 lobes. d:
541 raw noise, 6 lobes. This figure illustrates the impact of four different initial topographies. The plot
542 unveils a distinct pattern in the flow behaviour, characterized by backstepping of flows followed by
543 avulsion events, leading to the deposition of sediment in new locations. Each bar on the plot
544 represents the chronological order of flow deposits, ranging from the earliest to the latest. The
545 visualization provides valuable insights into the dynamic nature of sedimentation processes and the
546 influence of different initial topographies on the stacking patterns of beds.

547 Figure 10. Measurements of clustering and hierarchy in the four Lobyte3D models, plotted on top of
548 the synthetic fan model values. Note that Lobyte3D data points are plotted at the point on the x-axis
549 where, according to simple linear interpolation, the synthetic fan model would have the same
550 cluster strength value, assuming that the cluster strength is a reasonable measure of the degree of
551 randomness present in the bed centroid xy distribution. See text for discussion.

552

553

554

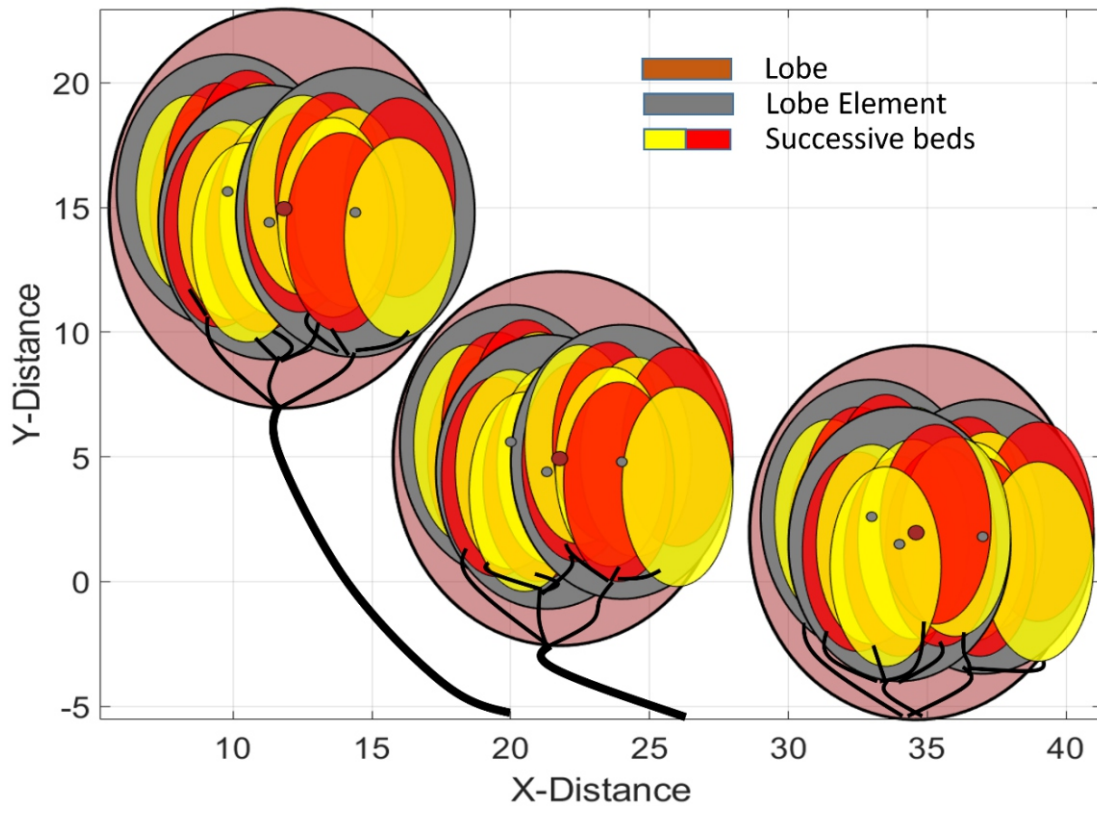
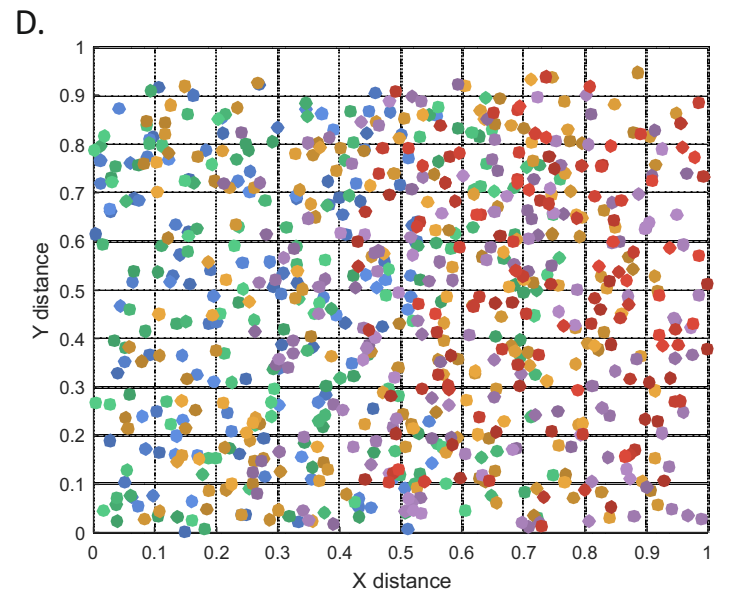
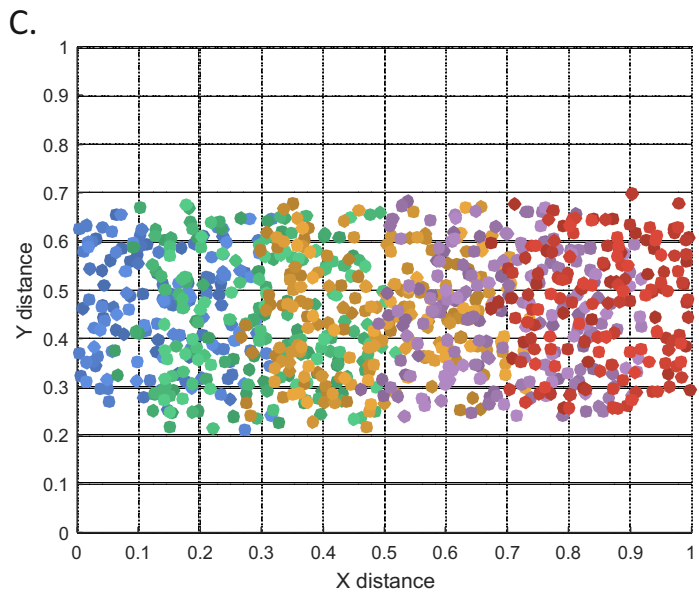
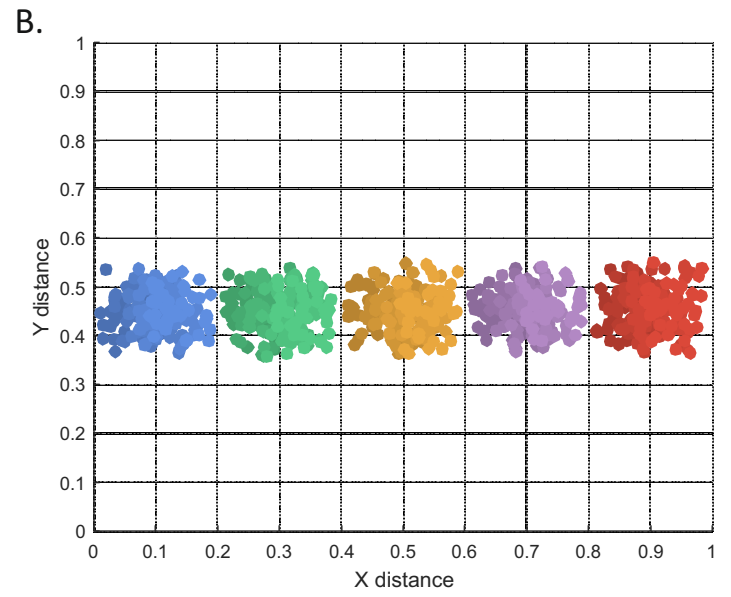
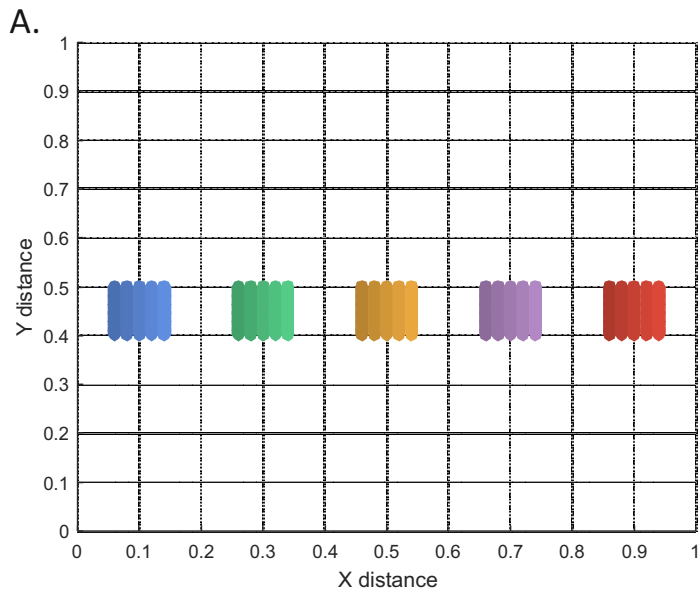
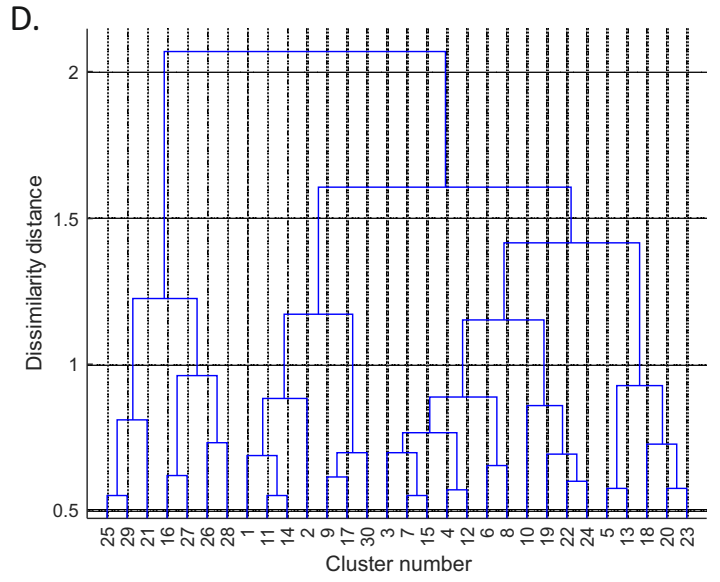
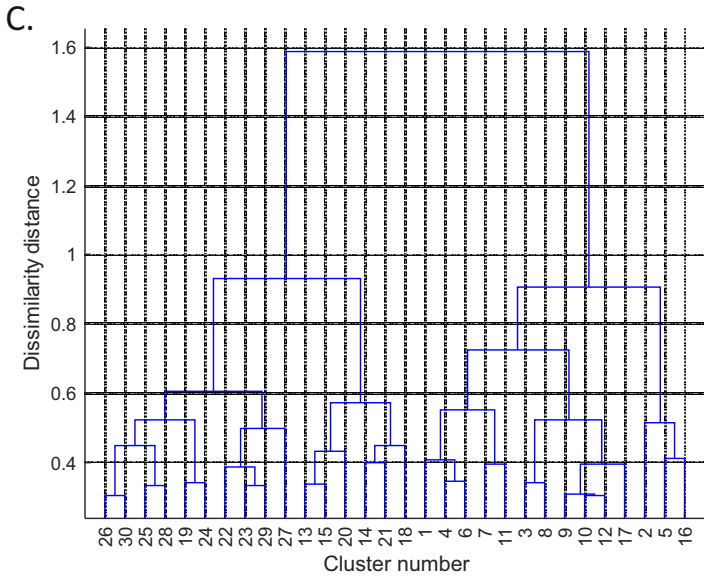
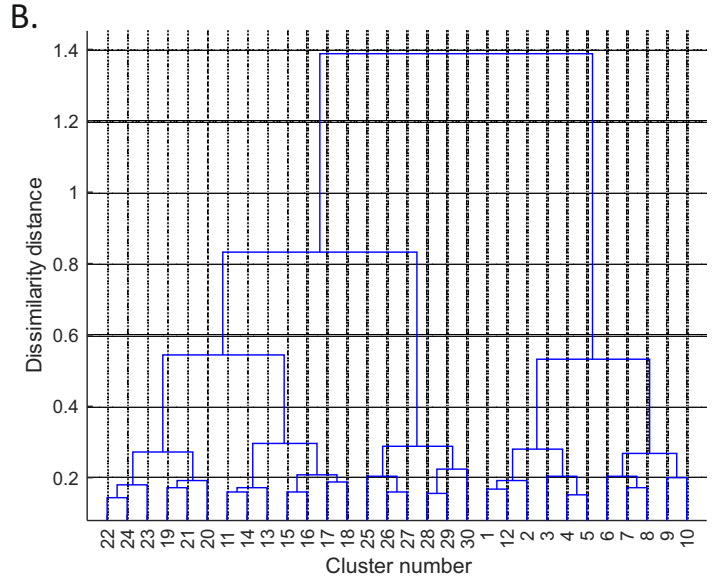
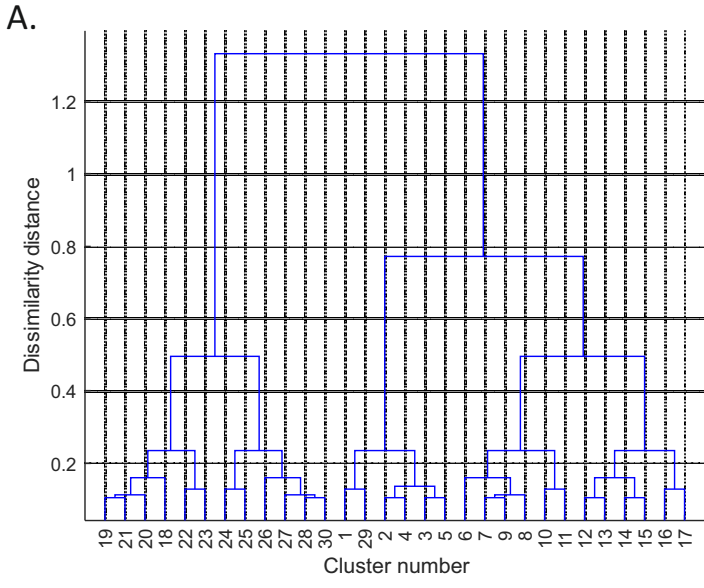
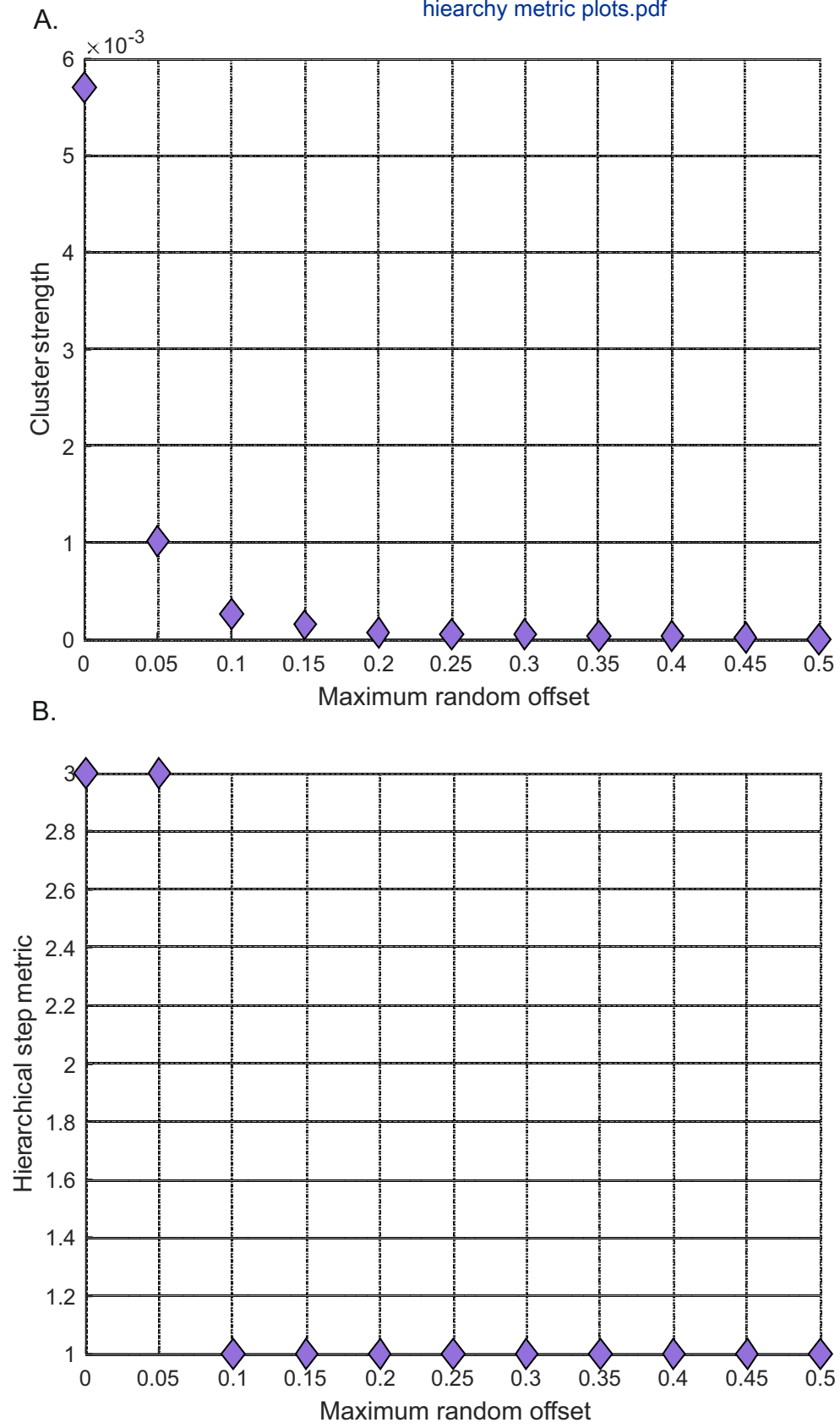


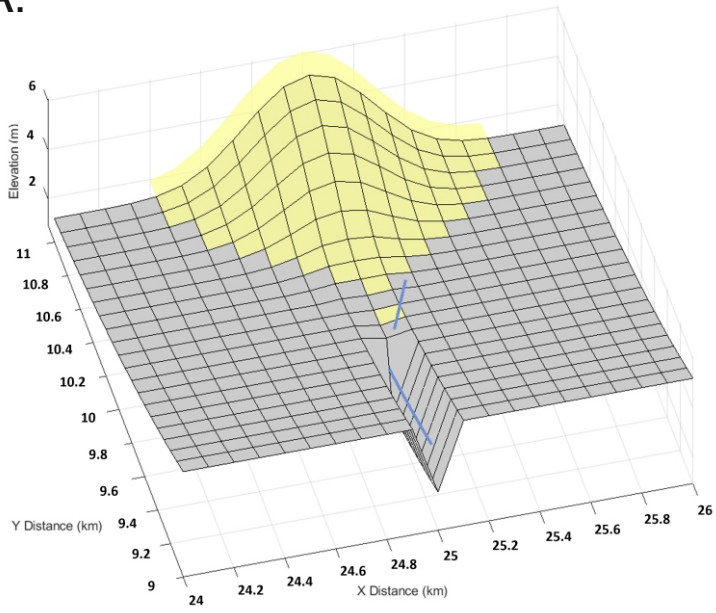
Figure 1



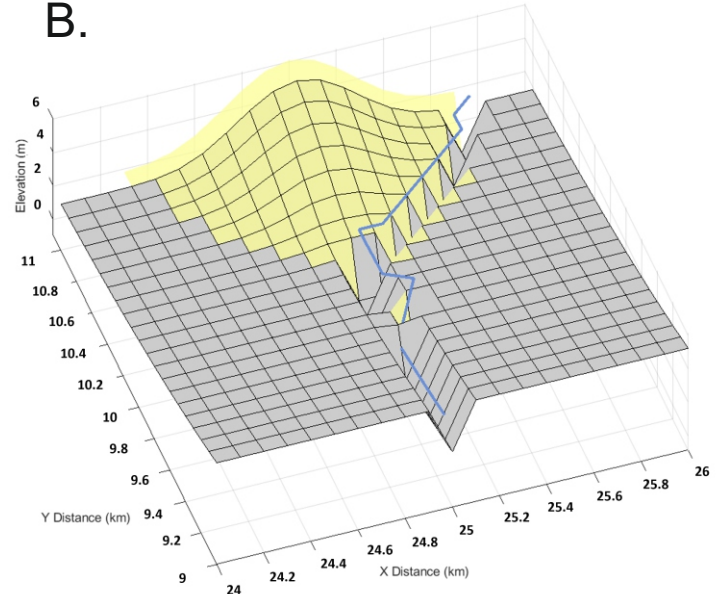


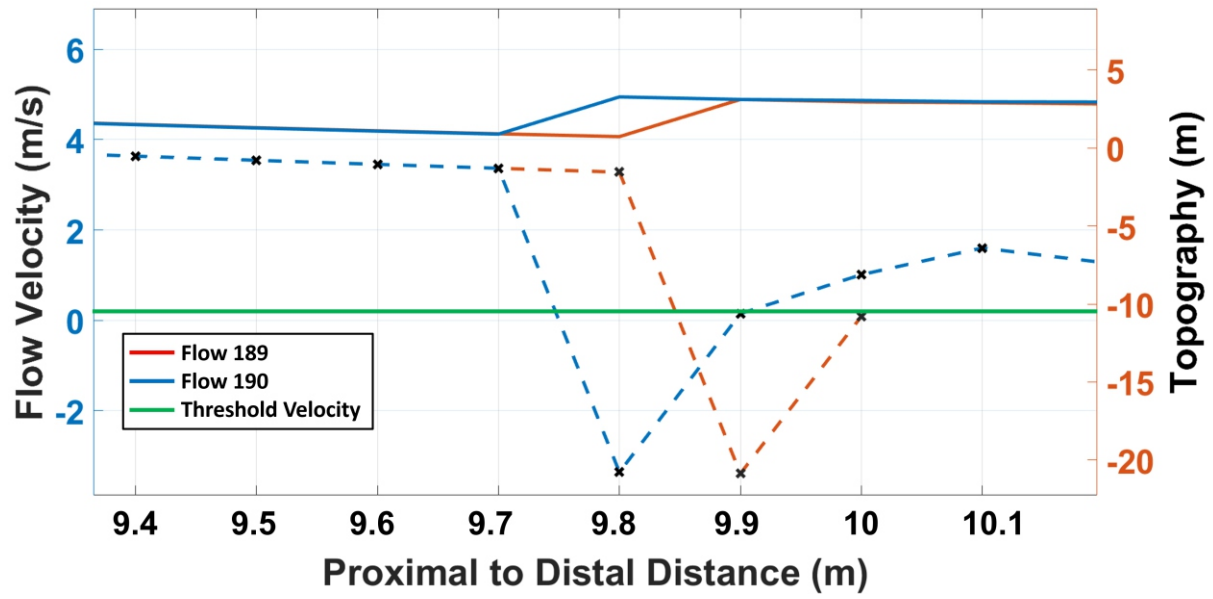


A.

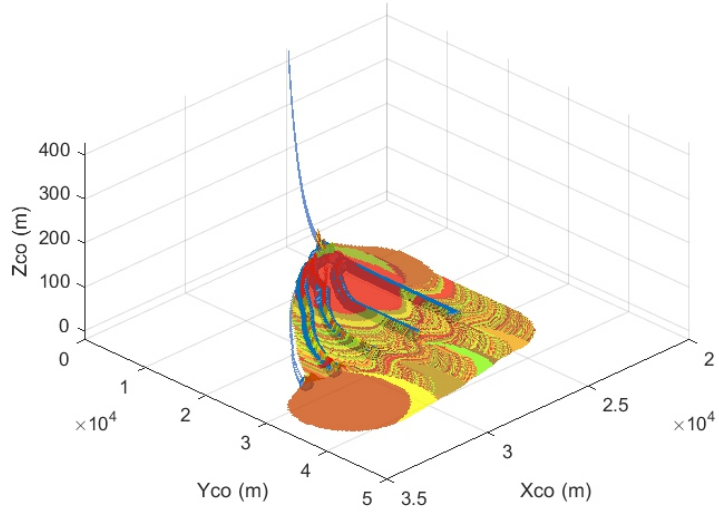


B.

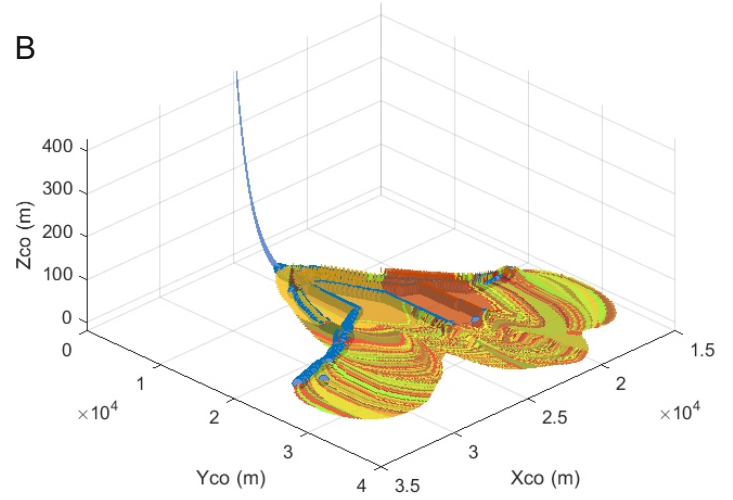




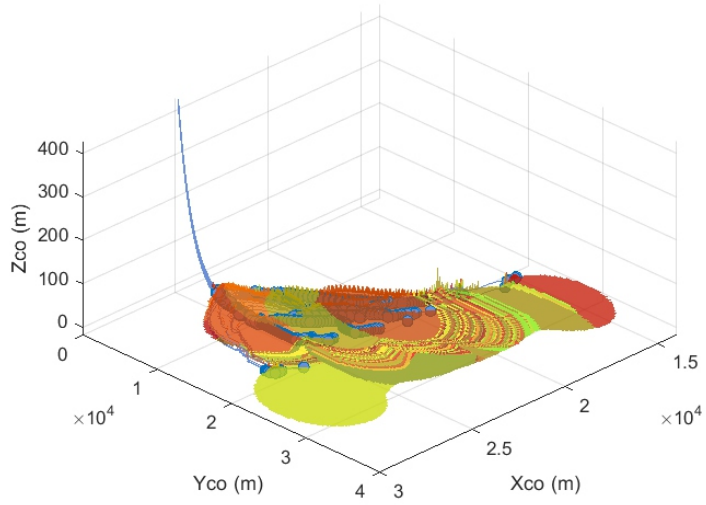
A



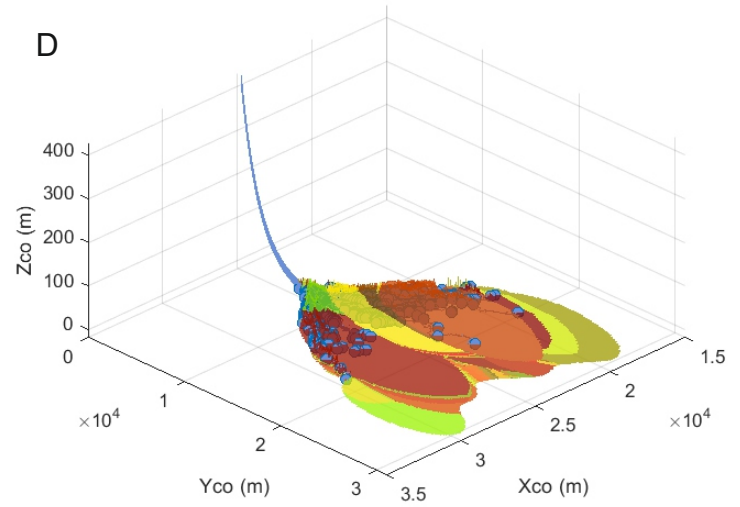
B

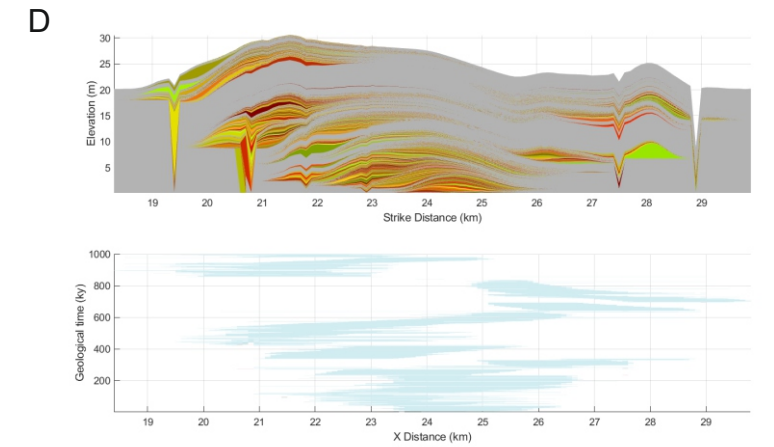
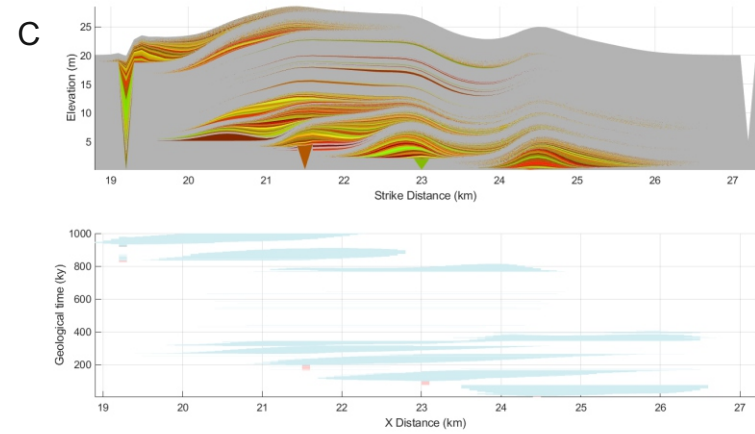
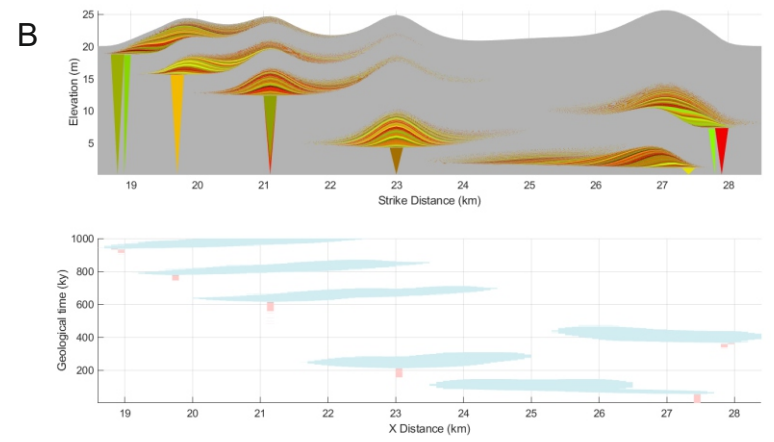
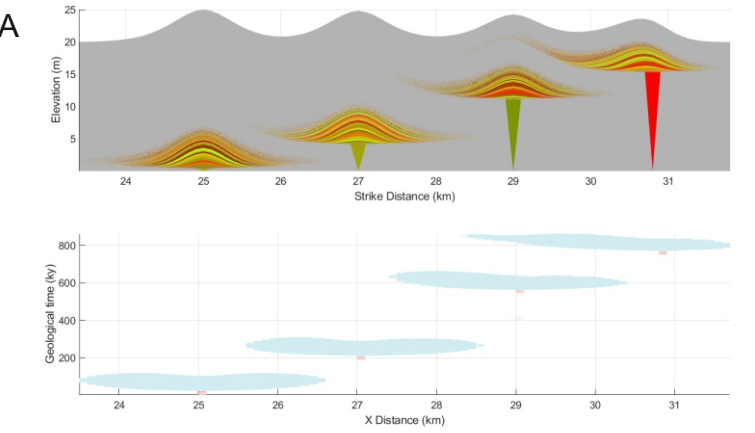


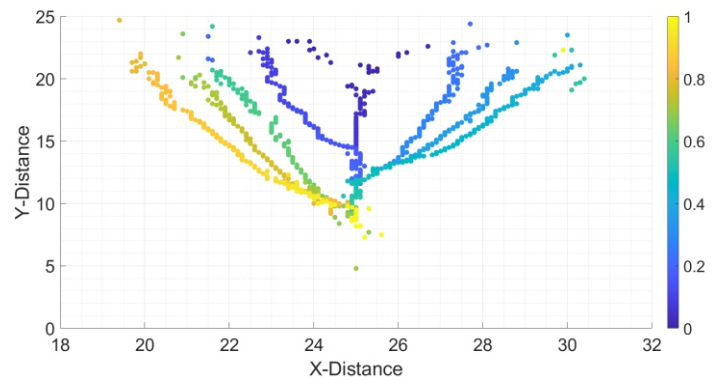
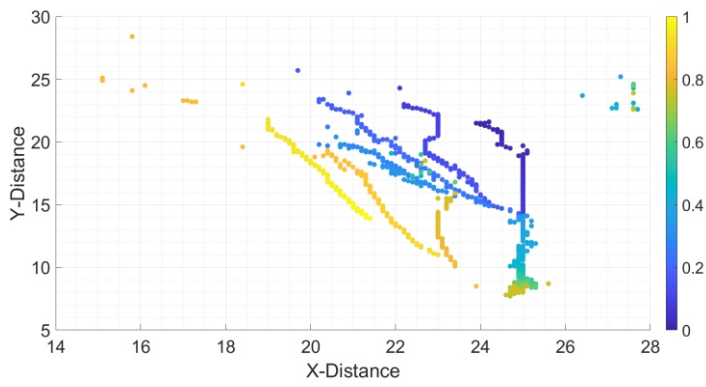
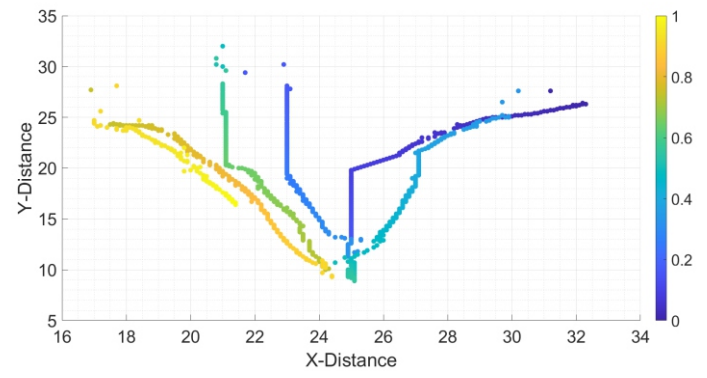
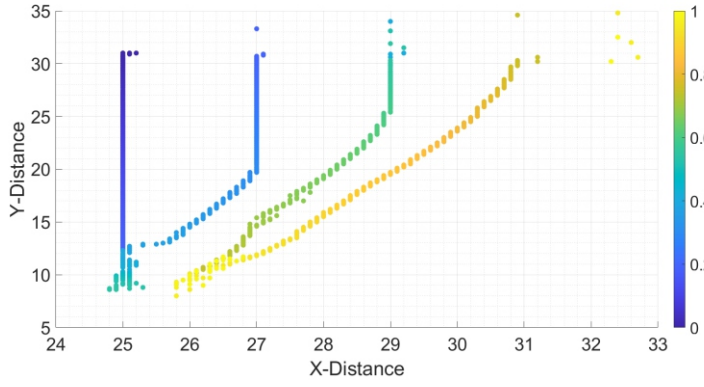
C



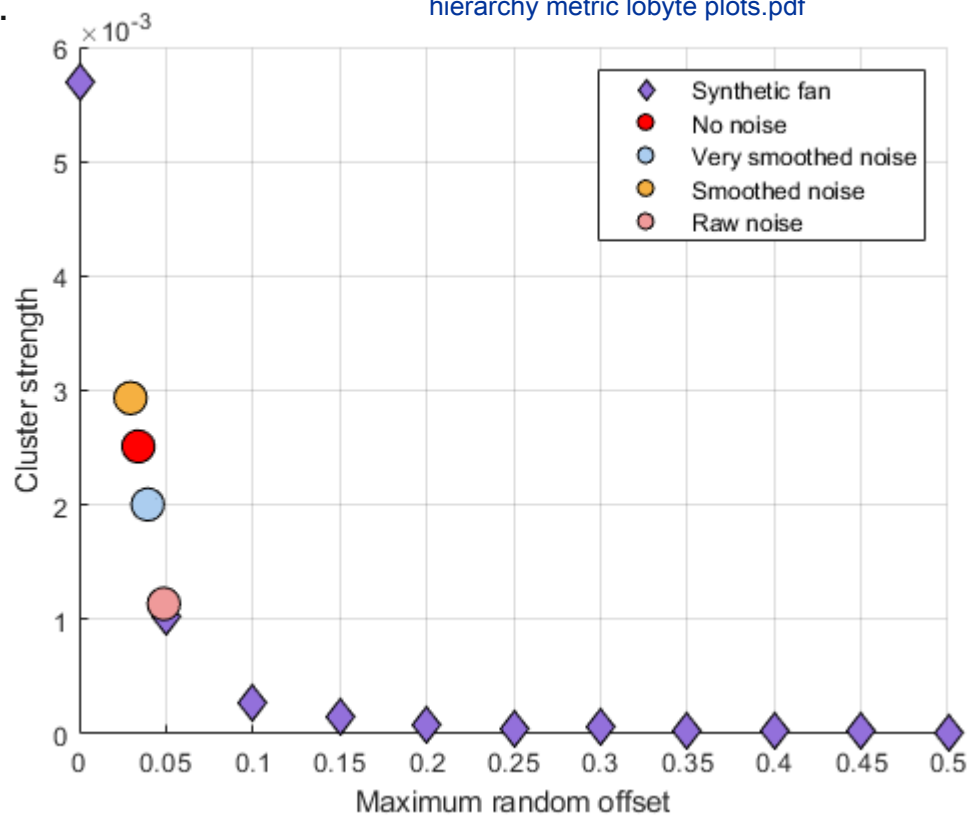
D







A.



B.

